Since January 2020 Elsevier has created a COVID-19 resource centre with free information in English and Mandarin on the novel coronavirus COVID-19. The COVID-19 resource centre is hosted on Elsevier Connect, the company's public news and information website.

Biosensors and Bioelectronics 183 (2021) 113206

Contents lists available at ScienceDirect

Biosensors and Bioelectronics

journal homepage: http://www.elsevier.com/locate/bios

Rapid and unamplified identification of COVID-19 with morpholino-modified graphene field-effect transistor nanosensor

Jiahao Li [a,1], Ding Wu [b,1], Yi Yu [a], Tingxian Li [a], Kun Li [a], Meng-Meng Xiao [c], Yirong Li [b,**], Zhi-Yong Zhang [c,***], Guo-Jun Zhang [a,*]

[a] School of Laboratory Medicine, Hubei University of Chinese Medicine, 16 Huangjia Lake West Road, Wuhan, 430065, PR China
[b] Department of Laboratory Medicine, Zhongnan Hospital of Wuhan University, 169 East Lake Road, Wuhan, 430071, PR China
[c] Hunan Institute of Advanced Sensing and Information Technology, Xiangtan University, Hunan, 411105, PR China

ARTICLE INFO

Keywords:
SARS-CoV-2
RdRp
Field-effect transistor
Amplification-free
Detection
Fast response

ABSTRACT

SARS-CoV-2 RNA is identified as a pivotal player to bolster energizing zones of COVID-19 detection. Herein, we develop a rapid and unamplified nanosensing platform for detection of SARS-CoV-2 RNA in human throat swab specimens. A gold nanoparticle (AuNP)-decorated graphene field-effect transistor (G-FET) sensor was fabricated, after which complementary phosphorodiamidate morpholino oligos (PMO) probe was immobilized on the AuNP surface. This sensor allowed for highly sensitive testing of SARS-CoV-2 RdRp as PMO does not have charges, leading to low background signal. Not only did the method present a low limit of detection in PBS (0.37 fM), throat swab (2.29 fM), and serum (3.99 fM), but also it achieved a rapid response to COVID-19 patients' samples within 2 min. The developed nanosensor was capable of analyzing RNA extracts from 30 real clinical samples. The results show that the sensor could differentiate the healthy people from infected people, which are in high agreement with RT-PCR results (Kappa index = 0.92). Furthermore, a well-defined distinction between SARS-CoV-2 RdRp and SARS-CoV RdRp was also made. Therefore, we believe that this work provides a satisfactory, attractive option for COVID-19 diagnosis.

1. Introduction

The outbreak of novel coronavirus disease (COVID-19) was declared a public health emergency of international concern (PHEIC), the highest level alarm, by the World Health Organization (WHO) on January 30, 2020. As of November 19, 2020, there had been nearly 56 million confirmed cases and more than one million deaths globally due to the rapid pandemic of severe acute respiratory syndrome coronavirus 2 (SARS-CoV-2) and the general, non-specific symptoms of this disease (Wang et al., 2020a). More seriously, compared to most previous epidemics, this infectious disease is much higher contagious because the spike (S) protein of SARS-CoV-2 shows overwhelming affinity with angiotensin-converting enzyme II (ACE2), which is abundantly expressed on the surface of human lung cells (Wrapp et al., 2020). There is no doubt that rapid detection and diagnosis are of key significance for disease treatment and outbreak control. Quantification and monitoring of viral loads are responsible for estimation of infection stage, and prediction of infectivity and recovery. Currently, the main detection techniques for COVID-19 in clinical laboratories can be broadly grouped into three categories: chest computed tomography (CT) scan, nucleic acid testing, and antibody testing (Ravi et al., 2020).

Viral RNA, generally, is a specific biomarker and tends to appear earlier than SARS-CoV-2 antibodies, which are produced by humoral immune response approximately a week or more after infection (Guo et al., 2020). And the antibody-producing capacity is weaker in immune-compromised human such as the elderly, children, and patients with immune-deficiency diseases, leading to a potentially false categorization or delayed diagnosis (Marsh and Orange 2019). Furthermore, immune cross-reactivity is an arduous conundrum in antibody testing. A recent study (Ng et al., 2020) confirmed the presence of pre-existing SARS-CoV-2 S protein-reactive antibodies in uninfected individuals. Collectively, based on current evidence, WHO does not recommend the

* Corresponding author.
** Corresponding author.
*** Corresponding author.
E-mail addresses: liyirong838@163.com (Y. Li), zyzhang@pku.edu.cn (Z.-Y. Zhang), zhanggj@hbtcm.edu.cn (G.-J. Zhang).
[1] These authors contributed equally to this work.

https://doi.org/10.1016/j.bios.2021.113206
Received 23 December 2020; Received in revised form 16 March 2021; Accepted 26 March 2021
Available online 30 March 2021

use of antigen or antibody-detecting rapid tests for clinical decision-making or diagnostic purposes. For these reasons, nucleic acid testing, such as reverse-transcription polymerase chain reaction (RT-PCR), loop-mediated isothermal amplification (LAMP), whole-genome sequencing, etc., are regarded as gold standards for diagnosis, with advantages of high specificity, favorable accuracy, and relatively short window period (Feng et al., 2020). In addition, quantitative detection of SARS-CoV-2 RNA plays an important role in early diagnosis, distinguishing COVID-19 and flu, evaluating treatment effect and prognosis.

However, RT-PCR, the main stream of molecular diagnosis, suffers from not only multistep processes but also a greater degree of human interaction, requiring expensive equipment and highly specialized laboratories. Thus it is still far from adequate because of quite a few limitations in high-throughput screening, point-of-care testing, as well as implementation in basic-level hospital (Tahamtan and Ardebili 2020). Furthermore, a crucial shortcoming of this technology lies in time-consuming. Long sample turn-around time increases the risk of transmission of COVID-19 to a wider community, and is not propitious for continuous monitoring, contact tracing and population screening. Although the efforts have never stopped to explore faster and more excellent methods, there is still an increasingly urgent demand for a rapid, effective, affordable and user-friendly testing strategy to diagnose COVID-19 timely and accurately.

Fortunately, in the age of rapid development of nanoscale science and technology, nanobiosensors, ideal solutions to neutralize the deficiencies of existing conventional methodologies, have shown vast fruits and superiority in the application of various biomolecules detection over the past decades (Talebian et al., 2020; Udugama et al., 2020; Weiss et al., 2020). At present, researchers have designed a multitude of biosensor-based nanoscale analytical tools and detection devices for COVID-19 diagnosis. Moitra et al., (2020) reported a gold nanoparticle-based colorimetric assay to detect SARS-CoV-2 N gene by "naked eye" without any expensive instrument. Another study (Qiu et al., 2020) from Switzerland detected SARS-CoV-2 RdRp gene by developing a cDNA-modified localized surface plasmon resonance (LSPR) biosensor combined with plasmonic photothermal effect, reaping a detection limit of 0.22 pM. Jiao et al., (2020) introduced a self-assembly DNA nanoscaffold into the hybrid chain reaction (HCR), proposing the "DNHCR" method that can amplify fluorescence signal of SARS-CoV-2 particular sequence 2-fold in comparison to conventional HCR with a detection limit of 0.96 pM. More recently, Yu and workers (Yu et al., 2020) manufactured a lateral flow strip which can test RdRp, N, and ORF3a gene simultaneously for multi-target detection of SARS-CoV-2. However, a noticeable drawback of this method was that it detected PCR products. In other words, pre-amplification by RT-PCR was a necessary condition for strip detection. Besides, there are plenty of other ingenious approaches and platforms conceived for SARS-CoV-2 detection, such as gel card agglutination assays (Alves et al., 2020), nanopore targeted sequencing (Wang et al., 2020b), cell-based biosensor (Mavrikou et al., 2020), etc. Nevertheless, these assays are still deficient in sensitivity, analysis time, or operability, and typically entail fluorescent markers or enzymatic labeling. Additionally, most of them only examined artificially synthesized sequences instead of biological specimen-derived viral RNA, failing to give a comprehensive picture for the practical application in clinical samples. Overall, they are not expected to address the clinical need in certain regards especially in an early phase of viral infection.

Among the variety of biosensors currently available, field-effect transistor (FET) biosensors, especially in combination with advanced functional nanomaterials (Ishikawa et al., 2009; Liang et al., 2020; Mei et al., 2018; Zhang et al., 2010), have been considered as ideal candidates for next-generation medical diagnostic platform (Syedmoradi et al., 2019), which allow the instant ultrasensitive detection while avoiding the dependence on various labelings. There is a consensus that graphene is one of the most renowned and attractive 2D semiconductor carbon nanosheets, owing to the atomic-level thickness, high carrier mobility, excellent conductivity, outstanding biocompatibility, and other unique properties (Zhang et al., 2019). In the past few years, graphene-based field-effect transistor (G-FET) biosensors have been widely reported to contribute to the diagnosis of many diseases, including heart failure, thrombotic events, tumors, as well as viral infectious diseases (Ishikawa et al., 2009; Lei et al., 2017; Wu et al., 2020; Yu et al., 2019; Zhang et al., 2016). Islam et al., (2019) detected human immunodeficiency virus (HIV) and its related diseases using G-FET biosensors functionalized with anti-p24 antibody. In one of our previous study (Jin et al., 2019), ebola virus, which can give rise to extremely serious diseases with a high mortality rate around 90%, was directly detected by a G-FET-based immunosensor. Of note, Seo et al., (2020) established a G-FET biosensing device to capture SARS-CoV-2 virus by the interactions between specific antibodies and S proteins. Given that only during active viral replication are the expressed antigens detected, the method hampers its real clinical applications in the inactive disease duration. Therefore, one of primary focus of future study should be continuing development of novel biosensors for SARS-CoV-2 nucleic acid testing, which is the definitive proof of COVID-19.

As widely emphasized in literatures, three conserved regions of SARS-CoV-2 genome are considered as the target sequences for detection among the available tests, which are the RdRp gene, N gene, and E gene. Similar to all RNA viruses, as is known, RdRp is the key player in genome replication and transcription of SARS-CoV-2. It is worth noting that the high conservation along the RdRp sequence was confirmed by comparing the alignment from SARS-CoV-2, SARS-CoV and MERS viruses (Buonaguro et al., 2020). Consequently, RdRp is considered as the most optimal target for detection and antiviral drugs.

In comparison of single-strand DNA (ssDNA) and peptide nucleic acid (PNA), PMO, an uncharged DNA analogue discovered by Summerton (Summerton and Weller 1997), possess exquisite specificity, long-term activity, nuclease-resistance, and length flexibility in hybridization events.

In this study, we design a AuNP-decorated G-FET nanosensor functionalized with PMO for rapid and unamplified identification of COVID-19, as diagrammed in Fig. 1. Taking advantage of the high surface-to-volume ratio of AuNP, and high stability, efficacy of PMO probe, trace amounts of SARS-CoV-2 RdRp gene can trigger a measurable shift of the Dirac point of the G-FET sensor upon hybridization of PMO with RdRp gene. Most critical of all, the nanosensor exhibits satisfying anti-interference ability and prospective clinical applicability by detecting SARS-CoV-2 RdRp in spiked biological sample (serum/throat swab) and 30 real clinical throat swab specimens. Besides, COVID-19 patients and non-COVID-19 individuals can be discriminated within 2 min in real-time measurement. Furthermore, the tedious, laborious process of RT-PCR amplification is circumvented, performing a high-speed direct detection without cumbersome manipulations.

2. Experimental section

2.1. Materials

Graphene oxide (GO) powders (99.99995%, 325 mesh) were bought from Alfa Aesar Co. Ltd. (Tianjin, China). 1-ethyl-3-(3-dimethyllaminopropyl) carbodiimide (EDC, 98%), N-hydroxysulfosuccinimide (sulfo-NHS, 98.5%), ethanolamine (EA), and RNaseZap were supplied by Sigma-Aldrich (Shanghai, China). Hydrazine (98%) and gold chloride trihydrate ($HAuCl_4 \cdot 3H_2O$) were purchased from Aladdin Co. Ltd. (Shanghai, China). Urea was obtained from Group Chemical Reagent Co. Ltd. (Shanghai, China). Thioglycolic acid (TGA, >95.0%) was gained from TCI Co. Ltd. (Shanghai, China). PMO used in this work was offered by Gene Tools LLC (Philomath, OR, USA). The HPLC-purified ssDNA probe and all selected RNAs, comprising SARS-COV-2 RdRp, SARS RdRp, non-complementary RNA, one-base mismatched RNA, and Cy3-labeled SARS-COV-2 RdRp were synthesized by Sangon Biotech

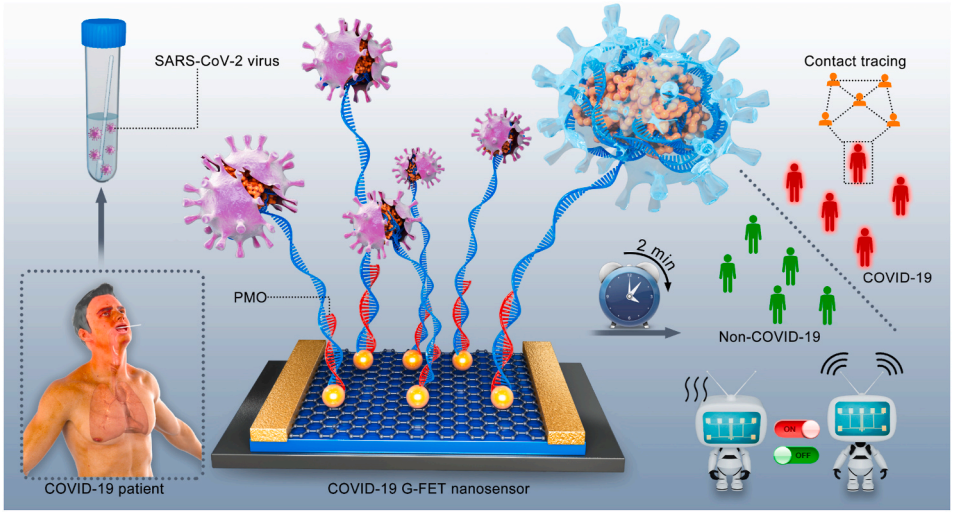

Fig. 1. Schematic diagram of PCR-free rapid direct identification of COVID-19 using the PMO-functionalized G-FET nanosensor.

(Shanghai, China). All oligonucleotide sequences involved in this work are listed in Table S1. 2019-nCoV nucleic acid detection kit (RT-PCR) was provided from bio-germ medical technology Co. Ltd. (Shanghai, China). Sodium dodecyl sulfate (SDS), nuclease-free phosphate buffer saline (PBS), and other chemicals were afforded by Generay Biotech Co. Ltd. (Shanghai, China). Ultrapure water, molecular biology grade, was applied to prepare all buffer solutions throughout the experiments involving hybridization.

Healthy human serum was obtained from Huangjia Lake Hospital of Hubei University of Chinese Medicine. Human throat swab specimens were collected from Zhongnan Hospital of Wuhan University. All clinical samples have been approved by the hospital ethics committee.

2.2. Fabrication of AuNP decorated G-FET sensors

The FET chip was produced by standard semiconductor technology as mentioned in our previous reports (Cai et al., 2014). In this work, the RGO was prepared by chemical reduction method with hydrazine, which is considered as standard reductant for GO. Hydrazine can effectively remove the oxygen-containing groups and make the atomic C/O ratio as high as 10.8 for RGO (Ambrosi A et al., 2012). Compared to electrical reduction, thermal reduction, and catalytic reduction, this approach is not only easy for operation, free of high temperature and high voltage, but also has high reduction degree (Ambrosi A et al., 2011). Then a diluted RGO (0.2 mg/mL) was drop-casted on the channel region and thermally annealed at 150 °C for 2 h. After that, the chip was sonicated with Piranha solution for 10 s to obtain few-layer RGO (step I). After treatment as mentioned before, the RGO FET sensor could be used for following functionalization. To obtain the AuNP-decorated G-FET device, 10 mM $HAuCl_4$ solution was immersed on the sensing nanochannel surface for 30 min to initiate the in-situ deposition of AuNP on the RGO (step II).

2.3. PMO immobilization

Afterwards, the chip was treated with a 0.5% TGA overnight to produce carboxylic group on the AuNPs surface through Au–S bonds (step III). Before PMO probe immobilization, the carboxylic group (-COOH) was activated by a solution prepared by mixing 0.1 M NHS and 0.4 M EDC in equal volume for 30 min. 10 μM PMO (10 μL) was subsequently introduced to the sensor chip and underwent 2h of incubation at room temperature (step IV). And then, the chip was washed three times with 1 × PBS containing 0.2% SDS, 1 × PBS and pure water, followed by 1h of incubation with 100 mM EA in order to eliminate possible nonspecific adsorption. The obtained device could be applied to subsequent detection.

2.4. Detection of SARS-CoV-2 RdRp

In the first place, the chip surface should be treated with RNaseZap before involving the hybridization with RNA. For SARS-CoV-2 RdRp detection, 10 μL of target RNA prepared with nuclease-free 1 × PBS at required concentration was incubated with the PMO-functionalized sensor chip at 37 °C for 30 min. Then the chip was subjected to stringent nuclease-free water flushing and drying with nitrogen flow.

2.5. Extraction of viral RNA from clinical samples

The total RNA from clinical throat swabs was extracted with a respiratory sample RNA isolation kit (Zhongzhi, Wuhan, China). Briefly, the taken throat swab samples were immediately immersed into 180 μL of virus preservation solution in a collection tube followed by being treated with 40 μL of cell lysates. And then, the collection tube was vortexed for 30s and maintained undisturbed for 30 min at room temperature. After a short centrifugation at 1000 RPM, the final suspension was applied for subsequent assays using RT-PCR and the COVID-19 G-FET nanosensor yielded in this work.

3. Results and discussion

3.1. Characterization of COVID-19 nanosensor device

The fabrication process of the COVID-19 nanosensor is shown in Fig. 2A. As depicted in this diagram, the successfully constructed sensing device experiences the deposition of gold nanoparticles and the immobilization of PMO probe.

To confirm that the COVID-19 G-FET nanosensor was ideally established, unambiguous characterization was performed after each step of functionalization. The scanning electron microscopy (SEM) image in Fig. 2B clearly presented a homogeneous and high density distribution of AuNPs on the RGO surface. And the mean particle diameter was around 10 nm. Because of the intensive van der Waals forces between AuNPs and RGO, the deposited AuNPs displayed a long-term stability in vacuum environments. Moreover, X-ray photoelectron spectroscopy (XPS) was used for further verification. The Au $4f_{7/2}$ (84.7 eV) and Au $4f_{5/2}$ (88.4 eV) peaks observed after step II (Fig. 2C) were attributed to the spontaneous AuNPs formation. The S_{2p} (164.5 eV) peak obtained after step III (Fig. 2D) indicated that AuNP surface successfully carried

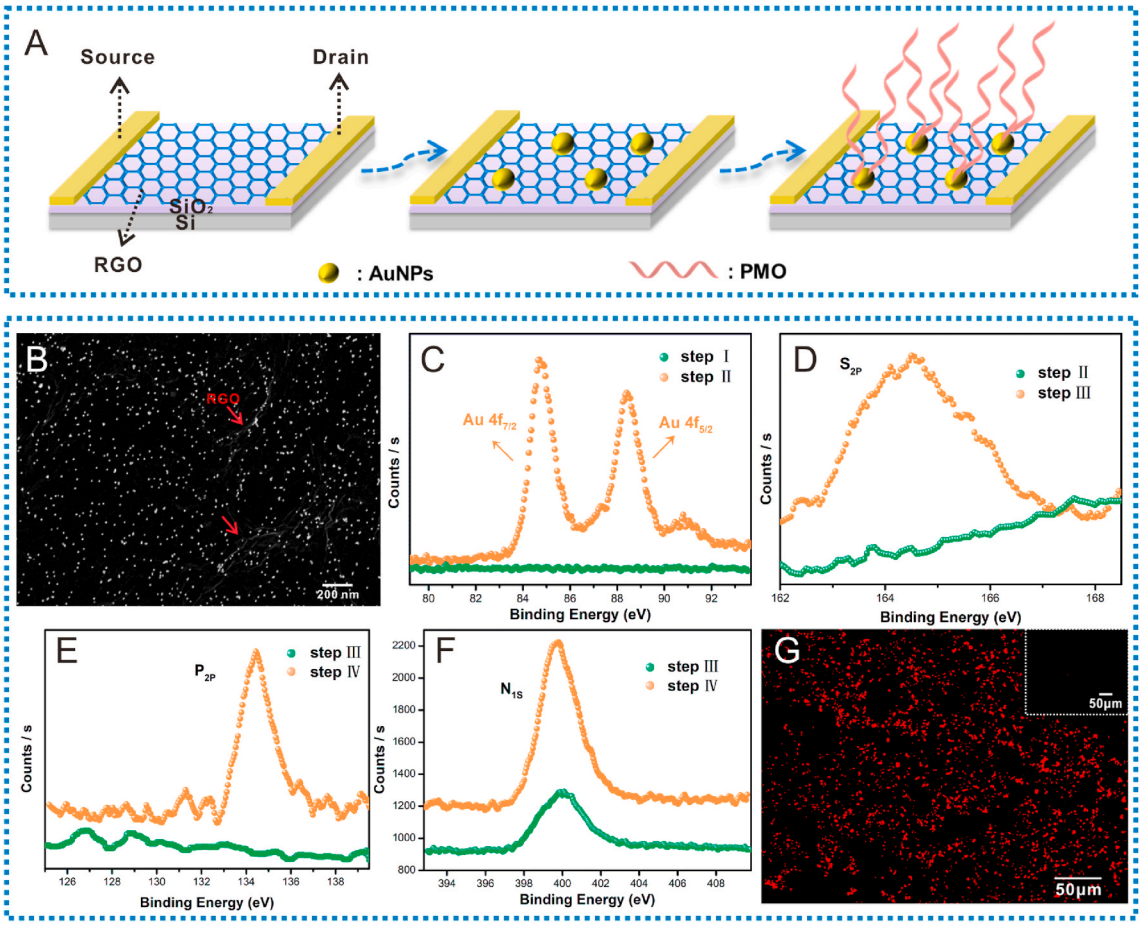

Fig. 2. Functionalization and characterization of the COVID-19 G-FET nanosensor. (A) Schematic illustration of surface functionalization for the device. (B) Scanning electron microscope image of AuNPs deposited onto RGO. Scale bars, 200 nm. (C–F) X-ray photoelectron spectroscopic spectra of Au, S, P, N elements, respectively. (G) Fluorescence image of a Cy 3-labeled SARS-CoV-2 RdRp hybridized to the PMO immobilized on G-FET channel surface. Scale bars, 50 μm.

carboxyl groups through Au–S bonds. To prove the successful modification of PMO probe, XPS spectra of P and N elements were analysed. As described in Fig. 2E, the appearance of P_{2p} (134.4 eV) peak after step Ⅳ corroborated the assembly of PMO probes. Furthermore, a sharp increment of the N_{1s} peak intensity at 399.8 eV (Fig. 2F) was expected from the content of N in PMO structure. And the low peak of N_{1s} in step III (green) was probably ascribed to N residues in hydrazine hydrate. The I_d-Vg transfer curves of the step-by-step functionalization procedure showed in Figure S1 further verified that the COVID-19 nanosensor was constructed successfully as anticipated. Consistent with the previous reported literature (Cai et al., 2014), AuNPs led to p-doping with a right shift of Dirac point (red line) compared to that of bare RGO curve (cyan line). While the negatively charged TGA induced n-doping (dark cyan line). Because PMO has a neutral backbone as mentioned above, the gate voltage of Dirac point showed negligible change after immobilization of PMO (purple line). Figure S2 shows the I_d-V_d characteristic curve, depicting clear evidence that the COVID-19 G-FET nanosensor revealed a behavior of p-type semiconductor.

Moreover, in order to confirm the successful hybridization between probe and SARS-COV-2 RdRp, target RNA labeled with Cy3 was incubated with the PMO-functionalized sensor chip for 30 min. After thoroughly rinsing step, the chip was imaged by fluorescence microscope. It can be obviously seen that a red fluorescence was gained in Fig. 2G, demonstrating the successful attachment of PMO and occurrence of expected hybridization events. Whereas, there was only a negligible signal in the control experiment (without PMO immobilization) that the chip underwent the same functionalization procedure, as shown in inset images.

3.2. Sensitivity and specificity

To study the sensitivity of the COVID-19 G-FET nanosensor for SARS-CoV-2 RdRp detection, a range of various concentrations of target RNA were tested by our device. By utilizing the semiconductor characterization system and a probe station to implement the electrical measurement of the sensor chip, the corresponding I_d-V_g curves were recorded. The measurements throughout drain current monitoring were performed in 0.01 × PBS as a liquid-gate and a bias of 0.1 V. An Ag/AgCl electrode was used as the gate to apply the liquid gate to stabilize the potential of the electrolyte. As revealed in Fig. 3A, as the concentration of target RNA enhanced from 1 fM to 100 pM, the Dirac point of ambipolar curves moved to the left gradually as a result of negative charge carried by RNA, which could generate a n-doping. ΔV_{CNP} means the variation of V_{CNP} after incubation (V_{CNP}, namely, the gate voltage of Dirac point), which is employed as the response signal. In detail, the mean values of $-\Delta V_{CNP}$ corresponding to diverse amounts of SARS-CoV-2 RdRp ranging from 1 fM to 100 pM also mounted up gradually, which were 29, 53, 69, 82, 107, and 124 mV, respectively. What is more, a good linear relationship with a high correlation coefficient value (R^2) of 0.998 between target RNA concentration and signal output was obtained as described in Fig. 3B. The regression equation was expressed as $-\Delta V_{CNP} = 18.64\ \lg C + 311.60$, in which C was the RNA concentration. The dashed line here was 3-fold of background signal (24 mV), which was produced by 1 × PBS. Combining the calibration curve in the Figure, a detection limit equal to 0.37 fM was obtained. The corresponding copy number concentration of the RdRp fragment was 223 copies/μL, which was calculated according to the following formula: copies/μL = 6.02 ×

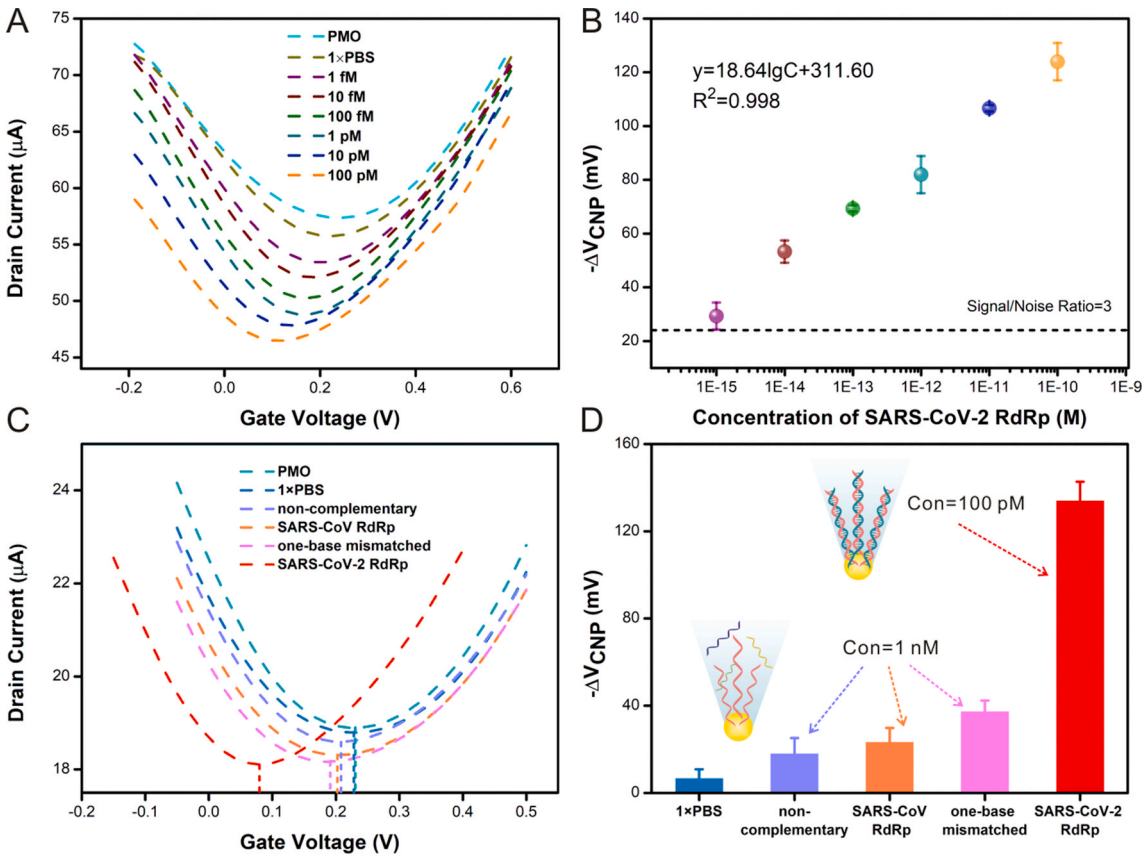

Fig. 3. Excellent analytical performance of COVID-19 G-FET nanosensor. (A) Transfer curves upon incubation with varying concentrations of SARS-CoV-2 RdRp (1 fM~100 pM). (B) Calibration curve at a series of target RNA concentrations (n = 3). The dashed line refers to 3-fold noise level. (C) Transfer curves upon incubation with PBS and nonspecific sequences including 1 nM non-complementary, SARS-CoV RdRp, and one-base mismatched RNA. (D) Variation of V_{CNP} at detection of blank and three nonspecific sequences.

10^{23} × concentration (g/μL)/(fragment length × 340). It is, moreover, noteworthy that our proposed method was 2–3 impressive orders of magnitude higher than another study (Qiu et al., 2020), in which SARS-CoV-2 RdRp was detected by LSPR with a LOD of 0.22 pM. Taking into account of the full-length of SARS-CoV-2 genome with 29.9 kilobases which is 1000 times as long as the RdRp-gene detected in this study, the sensitivity of our COVID-19 G-FET nanosensor can be further improved in detecting SARS-CoV-2 entire RNA strands, by reason of more negative charges carried by per target (Lin et al., 2009). According to literature reports, of note, the overall viral load of respiratory samples collected from 82 infected patients was higher than 1 × 10^3 copies/μL shortly after symptom onset (Pan et al., 2020), which considerably exceeds the above-mentioned detection limit (223 copies/μL). This illustrates that our sensing platform opens up the exciting possibility for directly detecting SARS-CoV-2 RNA from clinical samples with excellent sensitivity but without PCR amplification. We own this good performance to the high density of PMO immobilization, high efficiency of PMO-RNA hybridization, and high conductivity of RGO.

It is well known that one of the major challenges in SARS-CoV-2 detection lies in specificity, which is the prerequisite of a high degree of accuracy and the minimization of false positive. To investigate whether the developed COVID-19 nanosensor can distinguish between target RNA and non-specific sequences, 1 nM non-complementary RNA, 1 nM SARS-CoV RdRp, 1 nM one-base mismatched RNA, and 100 pM target RNA, namely SARS-CoV-2 RdRp, were successively exposed to the G-FET sensor chip, which had undergone entire functionalization process including AuNPs decoration and PMO attachment. The blank control experiment was first carried out by applying the same volume of 1 × PBS to the channel surface for 30 min. Fig. 3C depicts the transfer curves of the sensor chip after each incubation. Apparently, the Dirac point barely shifted after interaction with PBS and non-complementary RNA. And just only a negligible response, probably from nonspecific adsorption, appeared in the circumstances where SARS-CoV RdRp and one-base mismatched RNA were detected, whereas a remarkable shift of Dirac point was obviously observed in detection of SARS-CoV-2 RdRp. As summarized in Fig. 3D, in detail, the mean -ΔV_{CNP} values of three contaminant RNAs were calculated to be 6.7, 18, 23, and 37 mV, respectively. Differently, there was a dramatical variation of V_{CNP} in a lower concentration of SARS-CoV-2 RdRp, which was 5.8-fold of the response intensity of SARS-CoV RdRp. Of note, SARS-CoV and SARS-CoV-2 viruses present high similarities in RdRp sequences that only three fixed bases are different. Satisfyingly, it can be seen from Fig. 3C and D that our device held the power to discriminate between these two homologous beta-coronavirus accurately. Thus, it can be concluded that the developed assay enjoys high specificity for SARS-CoV-2 RNA testing.

3.3. Comparison of probe performances between PMO and ssDNA

To determine whether PMO is superior to ssDNA as an oligonucleotide probe and is more favorable for improving analytical performance, both sensitivity and selectivity of ssDNA-functionalized G-FET nanosensor were further examined. In this experiment, an amino-modified ssDNA probe with the same base sequence and concentration (10 μM) was used to replace PMO. As shown in Figure S3A and B, when detecting any given concentration of RdRp, the developed COVID-19 G-FET nanosensor gave rise to a more intensive signal output, while the -ΔV_{CNP} values of ssDNA-modified G-FETs were much smaller. Moreover, there was a significant difference ($P < 0.01$) in -ΔV_{CNP} values between these

two types of nanosensors for the same quantity of SARS-CoV-2 RdRp. Consistent with a study using PMO-functionalized silicon nanowire FETs for detection of DNA (Zhang et al., 2010), we find that the use of PMO as capture probes provides more responsive testing than ssDNA. We reason the favorable performance on sensitivity of our assay, probably arising from PMO-enhanced high affinity hybridization via the elimination of electrostatic repulsion between PMO-RNA duplex. Furthermore, to again compare the specificity, the measurements of blank, 1 nM non-complementary RNA, 1 nM SARS-CoV RdRp, and 1 nM one-base mismatched RNA were next carried out, respectively, with ssDNA-modified GFETs (Figure S3C). The corresponding $-\Delta V_{CNP}$ values were 8, 19.3, 36, and 49.3 mV as shown in Figure S3D. In terms of blank and non-complementary RNA detection, the response signal was negligible, which is similar to that of our developed device. When testing SARS-CoV RdRp and one-base mismatched RNA, nevertheless, the ssDNA-modified G-FETs generated greater spurious binding signal ($P < 0.05$), indicating a limited scope of discriminability between target RNA and a similar but not identical sequence. Particularly in case of that the content of endogenous interfering substances are relatively high in samples, the ssDNA-modified G-FETs are prone to false positive. To sum up, our proposed COVID-19 G-FET nanosensor harnessing PMO as capture probes is superior to the ssDNA-modified G-FETs in both sensitivity and specificity, and possesses greater potential for direct detection of SARS-CoV-2 in clinical samples.

3.4. Measurement of SARS-CoV-2 RdRp in throat swab and serum

We wonder whether our well-designed COVID-19 G-FET device could be used in real clinical samples which contain a complex matrix environment and multiple uncertain components. Therefore, the anti-interference capability against biological samples of our nanosensor was first verified prior to testing patient samples. In this experiment, throat swab and serum were selected for testing as diagramed in Fig. 4A. To better simulate the testing environment of clinical samples, the RdRp sequence with different concentrations (from 10 fM to 10 pM) were spiked into the 100% throat swab and undiluted serum from healthy individuals, respectively. The blank control here was incubated with same volume of throat swab or serum alone in the absence of target. As demonstrated in Fig. 4B–E, with the content of target RNA elevated from 10 fM to 10 pM, the sensing signal presented concentration-dependent enhancement with a linear relationship both in throat swab and serum detection. The regression equation were expressed as $-\Delta V_{CNP} = 12.255\lg C+205.416$ ($R^2 = 0.997$), and $-\Delta V_{CNP} = 12.074\lg C+203.852$ ($R^2 = 0.997$), respectively. On the basis of 3-fold of signal to noise ratio, the LOD was calculated to be 2.29 fM in throat swab, and 3.99 fM in serum. Moreover, Fig. 4F gives a more intuitive presentation and comparison. As we can see, although the sensing signals produced in throat swabs and serum were weaker than those in PBS at the same concentration of target, they were still significant and measurable response compared to background baseline (3-fold of blank), with satisfactory detection limits.

In addition, to further survey the repeatability and stability of our method, the recovery test was implemented as shown in Figure S4 and Table S2, where the average recovery rates ranged from 93.33% to 103.67%. These results suggest that our COVID-19 G-FET nanosensor has excellent anti-interference capability, accuracy and precision in biological samples analysis. It is known that throat swab is a commonly used upper respiratory specimen in SARS-CoV-2 screening. The feasibility of our device in throat swabs detection has critical implications in the practical applications in clinical patient samples. More interestingly, increasing studies reveal the existence of SARS-CoV-2 RNA in extrapulmonary sites, especially in serum. According to relevant reports (Chen et al., 2020a; Kim et al., 2020), detectable viral RNA in serum is a predictive indicator for clinical severity of COVID-19 patients, and is closely associated with the mortality rate, organ damage, and the level of interleukin 6 (IL-6), which may induce the occurrence of greater cytokine storms (Chen et al., 2020b). On the other hand, accurate detection of SARS-CoV-2 RNA in blood can effectively prevent the potential transfusion transmission. The good analysis ability of our nanosensor in serum, therefore, makes it attractive and versatile with a broad application prospect.

3.5. Clinical sample analysis with COVID-19 G-FET nanosensor

Most crucial of all, the practicability and validity of the COVID-19 G-FET nanosenser were verified in clinical samples by detecting a number

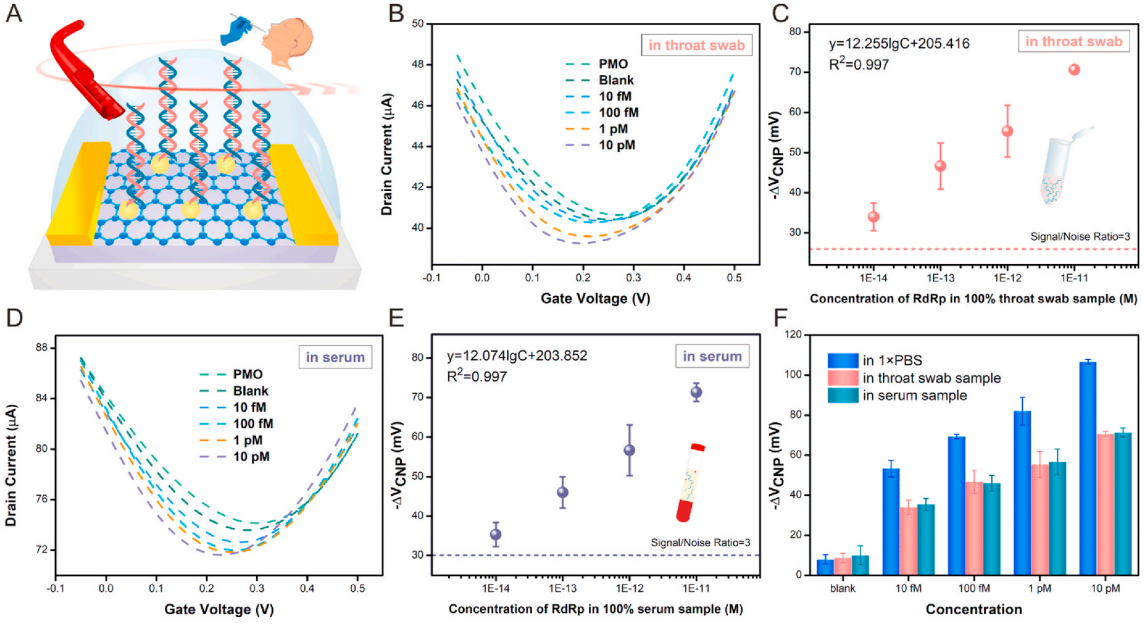

Fig. 4. Good anti-interference capability for RdRp detection in throat swabs and serum. (A) Schematic diagram of RdRp in throat swabs and serum specifically captured by the sensing region of the device. (B), (C) Transfer curves and variation of V_{CNP} at a series of concentrations (10 fM~10 pM) of target RNA in 100% throat swab sample from healthy person. (D), (E) Transfer curves and variation of V_{CNP} at a series of concentrations (10 fM~10 pM) of target RNA in 100% serum sample from healthy person. (F) Direct comparison of detection results in 1 × PBS, 100% throat swab sample and 100% serum sample by our method, respectively.

of heat-inactivated throat swab RNA extracts, from 20 confirmed patients and 10 excluded individuals, which had been tested by RT-PCR. With the same testing protocol as used in contrived reference samples in PBS, 10 μL of clinical samples was incubated with the biosensing interface for 30 min. According to the recorded transfer curves, the $-\Delta V_{CNP}$ values of each RNA extracts were calculated as presented in Fig. 5A–B. Overall, the average levels of sensing signal obtained from 20 COVID-19 patients were substantially higher than that of 10 healthy controls with a statistically significant difference ($p < 0.0001$). As clearly described in the heat map in Fig. 5C, the response of Dirac point variation was exceedingly intensive in RT-PCR positive cases but very weak in RT-PCR negative cases, signifying the well-defined distinction between the two groups. Additionally, to gain more insight about the diagnostic performance of our approach, the receiver operating characteristic curve (ROC) was applied. As we can see, an outstanding accuracy was reflected in Fig. 5D where the area under ROC was 0.995. Because the point closest to the top left corner of the ROC curve represents the fewest false positives and false negatives, the optimal cut-off value ($-\Delta V_{CNP} = 23$ mV) with a maximum positive likelihood ratio ($+LR = 10$) was acquired by software analysis. Based on these results, Kappa test was performed to evaluate the consistency between our method and the golden standard, ie, RT-PCR. Table S3 gives an explicit illustration that the Kappa index was 0.92, which means an almost perfect agreement. Hence, we draw the conclusions that our COVID-19 G-FET nanosensor has a high degree of reliability for direct detection of clinical samples, showing the good propensity to help overcome COVID-19.

3.6. Real-time detection of SARS-CoV-2 in clinical samples

For the sake of further reducing the detection time to realize rapid screening of COVID-19 patient, attempts in real-time dynamic response to clinical samples were performed. Briefly, the current between source and drain electrodes (I_{ds}) as a function of time was monitored under the gate voltage of −0.1 V upon injection of COVID-19 negative and positive samples, successively. As shown in Fig. 6A, the sensor device was only a slight drop in current during exposure with healthy sample. In contrast, a quite evident decline in current was observed after the addition of patient sample 8. As a result of the capture of negatively charged target sequence which led to an alteration of net carrier density on the channel surface, the I_{ds} signal decreased sharply within 2 min and then reached its saturation for about 300s (5 min) after injection. The current change rates of the two samples were shown in the inset histogram. Likewise, strong current responses were obtained in the detection of other patient samples as graphed in Fig. 6B–D. These results manifest the ability of our sensor to quickly detect SARS-CoV-2 RNA from clinical throat swabs within 2 min. In this analysis pattern, by measuring the I_{ds} in real-time, the developed nanosensor could determine who was infected or not in a trivial amount of time. Hence this method establishes an effective line of defense against the spread of pathogens and is paramount for timely public health surveillance.

To better assess the performance of our biosensor, we benchmarked LOD and detection time of the developed G-FET nanosensor in comparison with other SARS-CoV-2 RNA detection platforms (see Table S4), as shown in Fig. 6E. Overall, the established method in this work exhibits good performance in terms of LOD and detection time. Furthermore, the performance of different FET-based sensors for virus detection was also compared, as summarized in Table S5 and Fig. 6F. Although FET has previously made progress in the detection of many viruses, including HIV and HCV, etc., the proposed approach presents a more sensitive and rapid analysis. Undisputedly, this work provides new power and breakthrough for the application and development of FET biosensor in COVID-19 detection.

3.7. Reusability

Finally, the reusability of the device was interrogated, which is a considerable dimension for cost savings. In this verification experiment, PMO-RNA duplex was denatured by 8.3 M urea solution for 5 min. Afterwards, RdRp sequence (10 fM or 10 pM) was introduced to the chip surface once more. As such, 3 cycles of hybridization and dehybridization process were monitored as shown in Figure S5. The $-\Delta V_{CNP}$ values of the three times were 56, 54, 54 mV, respectively, in case of 10 fM target, and were 102, 100, 80 mV, respectively, in case of 10 pM target, indicating very close results with only slight changes. Thus, we hold the view that the fabricated nanosensor possesses good reusability and re-generability in both target detection with low and high concentration.

4. Conclusions

In this paper, we have established a PMO-functionalized G-FET nanosensor for the rapid direct detection of SARS-CoV-2 RNA in clinical throat swab samples with an attempt to realize a PCR-free identification of COVID-19. During the pandemic, this method is expected to be an effective diagnostic tool of COVID-19 with following attractive merits:

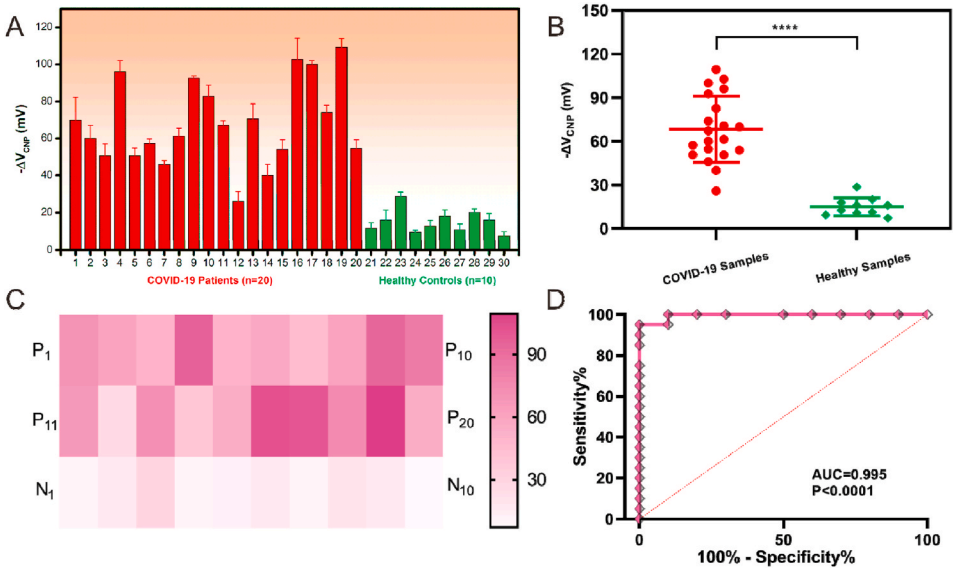

Fig. 5. COVID-19 G-FET nanosensor enables to detect SARS-CoV-2 RNA extracted from clinical throat swab samples. (A) Sensing signal in response to SARS-CoV-2 RNA from 20 COVID-19 patients and 10 healthy individuals. (B) Significant difference of signal among COVID-19 patients and the healthy individuals. (C) A heat map depicting the degree of Dirac point shift across 30 clinical samples. "Pn" indicates COVID-19 positive samples (n = 1–20), "Nn" indicates COVID-19 negative samples (n = 1–10). (D) ROC curve of COVID-19 G-FET nanosensor in response to SARS-CoV-2 RNA in clinical samples.

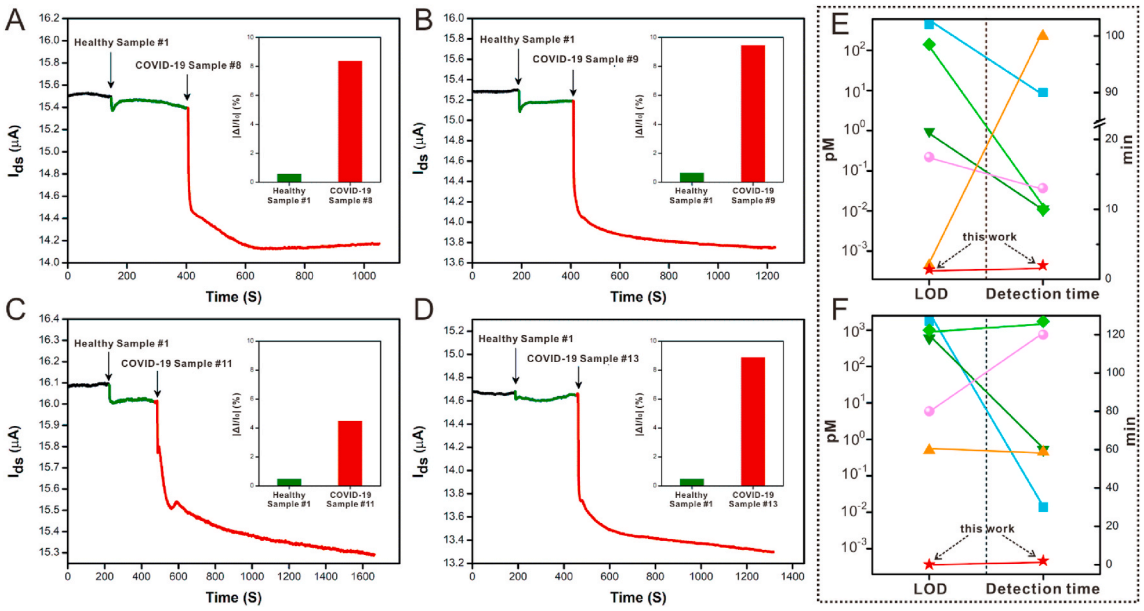

Fig. 6. Real-time electrical detection of clinical throat swabs from healthy individuals and COVID-19 patients. (A) Detection results of healthy sample 1 and COVID-19 sample 8. (B) Detection results of healthy sample 1 and COVID-19 sample 9. (C) Detection results of healthy sample 1 and COVID-19 sample 11. (D) Detection results of healthy sample 1 and COVID-19 sample 13. Insert: The current change rates of the two samples. (E) Benchmarking (by LOD and detection time) our nanosensor with other SARS-CoV-2 RNA detection platforms. (Reference data see Tables S4). (F) Benchmarking (by LOD and detection time) our nanosensor with previously reported FET-based biosensors for virus detection. (Reference data see Tables S5).

(i) Detection limit is as low as 0.37 fM, which is below the other reported biosensing platform (Table S4). (ii) Allowing a well-defined distinction between SARS-CoV-2 RdRp and SARS-CoV RdRp. (iii) Excellent anti-interference capability and precision in undiluted biological samples (throat swab/serum) detection. (iv) Outstanding reliability and accuracy for testing of RNA extracts from real clinical specimens and a high agreement with the results of RT-PCR. (v) Rapid specific response to COVID-19 patient samples can be achieved within 2 min by real-time measurement. (vi) A crucial advance in this work is PCR-free direct detection without pre-amplification, which consumedly reduces the molecular diagnostic turn-around time. In summary, the yielded platform provides a rapid (~2 min), sensitive, and reliable detection strategy for SARS-CoV-2. It is hoped that this sensing platform can be used as a rapid screening tool in the emergency department. When close contacts are under medical observation, the method can be used to quickly identify infected individuals and give immediate feedback to doctors. It is believed that this is a powerful means of combating current COVID-19 as well as any future outbreaks.

CRediT authorship contribution statement

Jiahao Li: Investigation, Visualization, Writing – original draft. **Ding Wu:** Methodology, Sample treatment. **Yi Yu:** Investigation. **Tingxian Li:** Investigation. **Kun Li:** Investigation. **Meng-Meng Xiao:** Chip fabrication. **Yirong Li:** Supervision, Sample treatment. **Zhi-Yong Zhang:** Supervision, Writing – review & editing. **Guo-Jun Zhang:** Supervision, Writing – review & editing, Project administration, Funding acquisition.

Declaration of competing interest

The authors declare that they have no known competing financial interests or personal relationships that could have appeared to influence the work reported in this paper.

Acknowledgements

This work was supported by the National Natural Science Foundation of China (No. 21974035).

Appendix A. Supplementary data

Supplementary data to this article can be found online at https://doi.org/10.1016/j.bios.2021.113206.

References

Ambrosi, A., Bonanni, A., Sofer, Z., Cross, J.S., Pumera, M., 2011. Electrochemistry at chemically modified graphenes. Chemistry 17 (38), 10763–10770.
Ambrosi, A., Chua, C.K., Bonanni, A., Pumera, M., 2012. Lithium aluminum hydride as reducing agent for chemically reduced graphene oxides. Chem. Mater. 24 (12), 2292–2298.
Alves, D., Curvello, R., Henderson, E., Kesarwani, V., Walker, J.A., Leguizamon, S.C., McLiesh, H., Raghuwanshi, V.S., Samadian, H., Wood, E.M., McQuilten, Z.K., Graham, M., Wieringa, M., Korman, T.M., Scott, T.F., Banaszak Holl, M.M., Garnier, G., Corrie, S.R., 2020. Rapid gel card agglutination assays for serological analysis following SARS-CoV-2 infection in humans. ACS Sens. 5 (8), 2596–2603.
Buonaguro, L., Tagliamonte, M., Tornesello, M.L., Buonaguro, F.M., 2020. SARS-CoV-2 RNA polymerase as target for antiviral therapy. J. Transl. Med. 18 (1), 158.
Cai, B., Wang, S., Huang, L., Ning, Y., Zhang, Z., Zhang, G.-J., 2014. Ultrasensitive label-free detection of PNA–DNA hybridization by reduced graphene oxide field-effect transistor biosensor. ACS Nano 8 (3), 2632–2638.
Chen, W., Lan, Y., Yuan, X., Deng, X., Li, Y., Cai, X., Li, L., He, R., Tan, Y., Deng, X., Gao, M., Tang, G., Zhao, L., Wang, J., Fan, Q., Wen, C., Tong, Y., Tang, Y., Hu, F., Li, F., Tang, X., 2020a. Detectable 2019-nCoV viral RNA in blood is a strong indicator for the further clinical severity. Emerg. Microb. Infect. 9 (1), 469–473.
Chen, X., Zhao, B., Qu, Y., Chen, Y., Xiong, J., Feng, Y., Men, D., Huang, Q., Liu, Y., Yang, B., Ding, J., Li, F., 2020b. Detectable serum severe acute respiratory syndrome coronavirus 2 viral load (RNAemia) is closely correlated with drastically elevated interleukin 6 level in critically ill patients with coronavirus disease 2019. Clin. Infect. Dis. 71 (8), 1937–1942.
Feng, W., Newbigging, A.M., Le, C., Pang, B., Peng, H., Cao, Y., Wu, J., Abbas, G., Song, J., Wang, D.-B., Cui, M., Tao, J., Tyrrell, D.L., Zhang, X.-E., Zhang, H., Le, X.C., 2020. Molecular diagnosis of COVID-19: challenges and research needs. Anal. Chem. 92 (15), 10196–10209.
Guo, L., Ren, L., Yang, S., Xiao, M., Chang, D., Yang, F., Dela Cruz, C.S., Wang, Y., Wu, C., Xiao, Y., Zhang, L., Han, L., Dang, S., Xu, Y., Yang, Q.-W., Xu, S.-Y., Zhu, H.-D., Xu, Y.-C., Jin, Q., Sharma, L., Wang, L., Wang, J., 2020. Profiling early humoral response to diagnose novel coronavirus disease (COVID-19). Clin. Infect. Dis. 71 (15), 778–785.
Ishikawa, F.N., Chang, H.-K., Curreli, M., Liao, H.-I., Olson, C.A., Chen, P.-C., Zhang, R., Roberts, R.W., Sun, R., Cote, R.J., Thompson, M.E., Zhou, C., 2009. Label-free, electrical detection of the SARS virus N-protein with nanowire biosensors utilizing antibody mimics as capture probes. ACS Nano 3 (5), 1219–1224.

Islam, S., Shukla, S., Bajpai, V.K., Han, Y.-K., Huh, Y.S., Kumar, A., Ghosh, A., Gandhi, S., 2019. A smart nanosensor for the detection of human immunodeficiency virus and associated cardiovascular and arthritis diseases using functionalized graphene-based transistors. Biosens. Bioelectron. 126, 792–799.

Jiao, J., Duan, C.J., Xue, L., Liu, Y.F., Sun, W.H., Xiang, Y., 2020. DNA nanoscaffold-based SARS-CoV-2 detection for COVID-19 diagnosis. Biosens. Bioelectron. 167, 112479.

Jin, X., Zhang, H., Li, Y.-T., Xiao, M.-M., Zhang, Z.-L., Pang, D.-W., Wong, G., Zhang, Z.-Y., Zhang, G.-J., 2019. A field effect transistor modified with reduced graphene oxide for immunodetection of Ebola virus. Mikrochim. Acta 186 (4), 223.

Kim, J.-M., Kim, H.M., Lee, E.J., Jo, H.J., Yoon, Y., Lee, N.-J., Son, J., Lee, Y.-J., Kim, M. S., Lee, Y.-P., Chae, S.-J., Park, K.R., Cho, S.-R., Park, S., Kim, S.J., Wang, E., Woo, S., Lim, A., Park, S.-J., Jang, J., Chung, Y.-S., Chin, B.S., Lee, J.-S., Lim, D., Han, M.-G., Yoo, C.K., 2020. Detection and isolation of SARS-CoV-2 in serum, urine, and stool specimens of COVID-19 patients from the Republic of Korea. Osong Public Health Res Perspect 11 (3), 112–117.

Lei, Y.M., Xiao, M.M., Li, Y.T., Xu, L., Zhang, H., Zhang, Z.Y., Zhang, G.J., 2017. Detection of heart failure-related biomarker in whole blood with graphene field effect transistor biosensor. Biosens. Bioelectron. 91, 1–7.

Liang, Y., Xiao, M., Wu, D., Lin, Y., Liu, L., He, J., Zhang, G., Peng, L.-M., Zhang, Z., 2020. Wafer-scale uniform carbon nanotube transistors for ultrasensitive and label-free detection of disease biomarkers. ACS Nano 14 (7), 8866–8874.

Lin, C.-H., Hung, C.-H., Hsiao, C.-Y., Lin, H.-C., Ko, F.-H., Yang, Y.-S., 2009. Poly-silicon nanowire field-effect transistor for ultrasensitive and label-free detection of pathogenic avian influenza DNA. Biosens. Bioelectron. 24 (10), 3019–3024.

Marsh, R.A., Orange, J.S., 2019. Antibody deficiency testing for primary immunodeficiency. Ann. Allergy Asthma Immunol. 123 (5), 444–453.

Mavrikou, S., Moschopoulou, G., Tsekouras, V., Kintzios, S., 2020. Development of a portable, ultra-rapid and ultra-sensitive cell-based biosensor for the direct detection of the SARS-CoV-2 S1 spike protein antigen. Sensors 20 (11), 3121.

Mei, J., Li, Y.-T., Zhang, H., Xiao, M.-M., Ning, Y., Zhang, Z.-Y., Zhang, G.-J., 2018. Molybdenum disulfide field-effect transistor biosensor for ultrasensitive detection of DNA by employing morpholino as probe. Biosens. Bioelectron. 110, 71–77.

Moitra, P., Alafeef, M., Dighe, K., Frieman, M.B., Pan, D., 2020. Selective naked-eye detection of SARS-CoV-2 mediated by N gene targeted antisense oligonucleotide capped plasmonic nanoparticles. ACS Nano 14 (6), 7617–7627.

Ng, K.W., Faulkner, N., Cornish, G.H., Rosa, A., Harvey, R., Hussain, S., Ulferts, R., Earl, C., Wrobel, A.G., Benton, D.J., Roustan, C., Bolland, W., Thompson, R., Agua-Doce, A., Hobson, P., Heaney, J., Rickman, H., Paraskevopoulou, S., Houlihan, C.F., Thomson, K., Sanchez, E., Shin, G.Y., Spyer, M.J., Joshi, D., O'Reilly, N., Walker, P. A., Kjaer, S., Riddell, A., Moore, C., Jebson, B.R., Wilkinson, M., Marshall, L.R., Rosser, E.C., Radziszewska, A., Peckham, H., Ciurtin, C., Wedderburn, L.R., Beale, R., Swanton, C., Gandhi, S., Stockinger, B., McCauley, J., Gamblin, S.J., McCoy, L.E., Cherepanov, P., Nastouli, E., Kassiotis, G., 2020. Preexisting and de novo humoral immunity to SARS-CoV-2 in humans. Science 370 (6522), 1339–1343.

Pan, Y., Zhang, D., Yang, P., Poon, L.L.M., Wang, Q., 2020. Viral load of SARS-CoV-2 in clinical samples. Lancet Infect. Dis. 20 (4), 411–412.

Qiu, G., Gai, Z., Tao, Y., Schmitt, J., Kullak-Ublick, G.A., Wang, J., 2020. Dual-functional plasmonic photothermal biosensors for highly accurate severe acute respiratory syndrome coronavirus 2 detection. ACS Nano 14 (5), 5268–5277.

Ravi, N., Cortade, D.L., Ng, E., Wang, S.X., 2020. Diagnostics for SARS-CoV-2 detection: a comprehensive review of the FDA-EUA COVID-19 testing landscape. Biosens. Bioelectron. 165, 112454.

Seo, G., Lee, G., Kim, M.J., Baek, S.-H., Choi, M., Ku, K.B., Lee, C.-S., Jun, S., Park, D., Kim, H.G., Kim, S.-J., Lee, J.-O., Kim, B.T., Park, E.C., Kim, S.I., 2020. Rapid detection of COVID-19 causative virus (SARS-CoV-2) in human nasopharyngeal swab specimens using field-effect transistor-based biosensor. ACS Nano 14 (4), 5135–5142.

Summerton, J., Weller, D., 1997. Morpholino antisense oligomers: design, preparation, and properties. Antisense Nucleic Acid Drug Dev. 7 (3), 187–195.

Syedmoradi, L., Ahmadi, A., Norton, M.L., Omidfar, K., 2019. A review on nanomaterial-based field effect transistor technology for biomarker detection. Microchim Acta 186 (11), 739.

Tahamtan, A., Ardebili, A., 2020. Real-time RT-PCR in COVID-19 detection: issues affecting the results. Expert Rev. Mol. Diagn 20 (5), 453–454.

Talebian, S., Wallace, G.G., Schroeder, A., Stellacci, F., Conde, J., 2020. Nanotechnology-based disinfectants and sensors for SARS-CoV-2. Nat. Nanotechnol. 15 (8), 618–621.

Udugama, B., Kadhiresan, P., Kozlowski, H.N., Malekjahani, A., Osborne, M., Li, V.Y.C., Chen, H., Mubareka, S., Gubbay, J.B., Chan, W.C.W., 2020. Diagnosing COVID-19: the disease and tools for detection. ACS Nano 14 (4), 3822–3835.

Wang, D., Hu, B., Hu, C., Zhu, F., Liu, X., Zhang, J., Wang, B., Xiang, H., Cheng, Z., Xiong, Y., Zhao, Y., Li, Y., Wang, X., Peng, Z., 2020a. Clinical characteristics of 138 hospitalized patients with 2019 novel coronavirus–infected pneumonia in wuhan, China. J. Am. Med. Assoc. 323 (11), 1061–1069.

Wang, M., Fu, A., Hu, B., Tong, Y., Liu, R., Liu, Z., Gu, J., Xiang, B., Liu, J., Jiang, W., Shen, G., Zhao, W., Men, D., Deng, Z., Yu, L., Wei, W., Li, Y., Liu, T., 2020b. Nanopore targeted sequencing for the accurate and comprehensive detection of SARS-CoV-2 and other respiratory viruses. Small 16 (32), e2002169.

Weiss, C., Carriere, M., Fusco, L., Capua, I., Regla-Nava, J.A., Pasquali, M., Scott, J.A., Vitale, F., Unal, M.A., Mattevi, C., Bedognetti, D., Merkoçi, A., Tasciotti, E., Yilmazer, A., Gogotsi, Y., Stellacci, F., Delogu, L.G., 2020. Toward nanotechnology-enabled approaches against the COVID-19 pandemic. ACS Nano 14 (6), 6383–6406.

Wrapp, D., Wang, N., Corbett, K.S., Goldsmith, J.A., Hsieh, C.-L., Abiona, O., Graham, B. S., McLellan, J.S., 2020. Cryo-EM structure of the 2019-nCoV spike in the prefusion conformation. Science 367 (6483), 1260–1263.

Wu, D., Yu, Y., Jin, D., Xiao, M.M., Zhang, Z.Y., Zhang, G.J., 2020. Dual-aptamer modified graphene field-effect transistor nanosensor for label-free and specific detection of hepatocellular carcinoma-derived microvesicles. Anal. Chem. 92 (5), 4006–4015.

Yu, S., Nimse, S.B., Kim, J., Song, K.-S., Kim, T., 2020. Development of a lateral flow strip membrane assay for rapid and sensitive detection of the SARS-CoV-2. Anal. Chem. 92 (20), 14139–14144.

Yu, Y., Li, Y.-T., Jin, D., Yang, F., Wu, D., Xiao, M.-M., Zhang, H., Zhang, Z.-Y., Zhang, G.-J., 2019. Electrical and label-free quantification of exosomes with a reduced graphene oxide field effect transistor biosensor. Anal. Chem. 91 (16), 10679–10686.

Zhang, C., Xu, J.Q., Li, Y.T., Huang, L., Pang, D.W., Ning, Y., Huang, W.H., Zhang, Z.Y., Zhang, G.J., 2016. Photocatalysis-induced renewable field-effect transistor for protein detection. Anal. Chem. 88 (7), 4048–4054.

Zhang, G.J., Luo, Z.H., Huang, M.J., Tay, G.K., Lim, E.J., 2010. Morpholino-functionalized silicon nanowire biosensor for sequence-specific label-free detection of DNA. Biosens. Bioelectron. 25 (11), 2447–2453.

Zhang, Y.Y., Wan, Q.J., Yang, N.J., 2019. Recent advances of porous graphene: synthesis, functionalization, and electrochemical applications. Small 15 (48), e1903780.